





Probing an auxiliary laser to tune the repetition rate of a soliton microcomb

TANVIR MAHMOOD,^{1,*}  JAMES P. CAHILL,¹ PATRICK SYKES,^{1,2}
LOGAN COURTRIGHT,² LUE WU,³  KERRY J. VAHALA,³  CURTIS
R. MENYUK,²  AND WEIMIN ZHOU¹

¹DEVCOM Army Research Laboratory, 2800 Powder Mill Road, Adelphi, MD 20783, USA

²University of Maryland, Baltimore County, 1000 Hilltop Circle, Baltimore, MD 21250, USA

³T. J. Watson Laboratory of Applied Physics, California Institute of Technology, Pasadena, CA 91125, USA

*tanvir.mahmood.civ@army.mil

Abstract: We demonstrate that it is possible to linearly tune the repetition rate of a bright soliton comb that is generated using an Si₃N₄ microring resonator by linearly varying the frequency of an auxiliary heater laser. Hence, the auxiliary laser can be utilized as a linear active feedback element for stabilizing the repetition rate. We investigated the potential of the auxiliary laser as an actuator of the soliton repetition rate by varying the auxiliary laser frequency at different modulation rates. Within the modulation bandwidth of the laser, we find that the variation ratio, defined as the ratio of the change in the repetition rate to the change in the laser frequency, remains unchanged. This variation ratio also quantifies the correlation between the frequency drift of the auxiliary laser and the repetition rate phase noise and makes it possible to examine the impact of frequency drift on the attainable phase noise performance of the soliton microcomb. For our setup, we find that the repetition rate phase noise of the microcomb below a 1-kHz offset from the carrier is dominated by the frequency drift of the auxiliary laser, which emphasizes the importance of deploying an inherently low-phase-noise laser when auxiliary laser heating technique is utilized.

© 2025 Optica Publishing Group under the terms of the [Optica Open Access Publishing Agreement](#)

1. Introduction

Generating temporal dissipative Kerr solitons (DKSs) in the anomalous dispersion regime of the high- Q microresonator devices is a widely adopted technique to implement chip-scale optical frequency combs (OFCs), also known as microcombs. Based on strong light interaction with the third order Kerr ($\chi^{(3)}$) nonlinearity of the medium, such OFCs have been demonstrated in a growing number of highly nonlinear material platforms, including silica (SiO₂) [1–3], silicon nitride (Si₃N₄) [4–8], magnesium fluoride (MgF₂) [9], aluminum-gallium arsenide (AlGaAs) [10,11], tantalum (Ta₂O₅) [12] and many more [13–15]. Owing to the design flexibility, dispersion engineering capability, and large transparent window, DKS formations in these photonic devices make it possible to achieve fully-coherent, broadband microcombs that can enable chip-scale, low-phase-noise frequency sources in the frequency range of gigahertz to terahertz [16–18]. However, accessing stable DKSs in practice is experimentally challenging due to the thermal instability. In a two-dimensional stability map of the pump power and cavity-pump detuning, the stable DKS regions are accessible when the pump laser is red-detuned relative to the thermally- and Kerr-shifted cavity [19]. As the pump laser is swept from blue to red-detuned regime with respect to the resonance, the microresonator transits through a parameter range in which the modulation instability occurs, and the intracavity power experiences step-like abrupt drops during DKS transitions. As a result, the cavity resonance shifts towards higher frequency owing to cooling of the resonance corresponding to the thermal drift. Consequently, the cavity-pump detuning increases beyond the stable DKS existence region, leading to extinction of the desired soliton state. Several techniques have been explored to overcome this challenge, including precise

adjustment of the pump frequency scanning rate [9], power kicking [1], fast scanning with an SSB-SC frequency shifter [3], thermal tuning using a micro-heater [20], and auxiliary laser heating [21–26]. In the auxiliary laser heating technique, the thermal drift that occurs during DKS transitions is mitigated by coupling a second laser, in addition to the pump laser, into the cavity. The heat, resulting from the absorption of the circulating light from the auxiliary laser, continuously compensates for the thermal instability in the cavity and thereby allows the pump laser to stably access the DKS regime. In this work, we probe the effectiveness of this technique to both stably access the DKS existence region and tune the repetition rate of the resulting microcomb. We demonstrate that it is possible to linearly tune the repetition rate of a bright soliton comb that is generated using an Si_3N_4 microring resonator by linearly varying the frequency of an auxiliary heater laser. This linear variation can be used as an actuator to tune the repetition rate. This linear variation also implies that laser frequency noise will linearly perturb the soliton repetition rate and hence may set a lower limit to the phase-noise performance of the soliton frequency comb, which we observed in our setup.

One of the advantages of using an auxiliary laser in the generation of a DKS microcomb is that this approach reduces the dependence on precise control of the scanning rate and eliminates the need for an abrupt change in the pump power and frequency. The pump laser can be scanned at a slow speed to the red-detuned side of the pump resonance, and the abrupt shift in the intracavity power during the transition to DKS states is continuously compensated by the auxiliary laser, which is coupled into a second high- Q resonance and remains on the blue side of its own resonance. Consequently, the soliton survival time in the microresonator cavity increases, and the desired soliton state or corresponding microcomb can last for hours without active feedback locking. However, the free-running repetition rate of the soliton microcomb exhibits higher intrinsic phase noise than conventional radio-frequency (RF) oscillators do. One of the sources, contributing to the increased phase noise, is the laser frequency drift that causes fluctuations in the detuning between the pump laser and its corresponding cavity resonance [1]. Laser self-injection locking (SIL) can alleviate this issue by means of the Rayleigh back-scattered light to lock the cavity-pump detuning [4]. However, the technique requires a meticulous control of the gap between the pump laser facet and the device ingress for the precise adjustment of the feedback phase. The thermal and coupling variations [18] as well as the thermo-refractive noise [27] can also affect the repetition rate phase noise. The persistent balancing of the intracavity power, provided by including an auxiliary laser in the system, continuously counters these effects and thereby mitigates the drift of the repetition rate of the microcomb.

For low-phase-noise RF synthesis and precision metrology, further stabilization of the carrier envelope offset (f_{ceo}) and the repetition rate (f_{rep}) of the microcomb is necessary. Recently a passive f_{rep} stabilization mechanism has been demonstrated by injecting a low-phase-noise secondary light source into the cavity, whereby f_{rep} can be locked to another optical reference via Kerr injection locking [28–30]. Although the simplicity of such passive schemes can be advantageous, the use of active feedback may still be desirable in some cases. Active stabilization mechanisms that rely solely on the pump laser properties couple the individual feedback actuations of f_{ceo} and f_{rep} to each other. For example, the f_{ceo} can be stabilized by using the pump laser frequency (f_{pump}) as an actuator; however, modifying f_{pump} also affects the cavity-pump detuning and perturbs f_{rep} through thermal heating and the Kerr effect. Stabilizing f_{rep} by actively controlling f_{pump} is also common [31–33], however it couples with the f_{ceo} via the relation, $f_{\text{ceo}} = f_{\text{pump}} - N \times f_{\text{rep}}$, where N is a positive integer. Conversely, f_{rep} can be stabilized using the pump amplitude as an actuator [3,34,35]. When a distributed feedback (DFB) laser operates as the pump, actuating the pump amplitude also changes the frequency of the laser, and leads to undesirable cross-talk between the actuation of f_{rep} and f_{ceo} . It is preferable to have two independent “knobs” to stabilize both the f_{ceo} and the f_{rep} . Without affecting f_{ceo} , the stabilization of f_{rep} can be implemented orthogonally by using metallic heaters around the

microresonator device [20,36] or installing a thermoelectric cooler (TEC) underneath the device to regulate the cavity round-trip time via heating [32]. The stabilization process using a TEC is slow and is subject to the bulk response of the material stack since the TEC operates far from the core material layer. The resistive metal layer stack is also required to be sufficiently far from the device core to avoid increasing the propagation loss and degrading the device performance. This constraint limits the efficiency of the resistive heating, heat localization, and effective bandwidth of the feedback actuation. Furthermore, the heat capacity of the metal layer decreases as the system temperature approaches to zero, so that it cannot be used with microcombs that operate at cryogenic temperatures. Mechanical actuation techniques have also been used to stabilize f_{rep} [37–39]. This approach relies on a piezoelectric material (e.g. AlN, ZnO) coating that adjusts the stress that is induced on the microresonator device by changing the applied voltage. Although this approach makes it possible to tune f_{rep} over a larger bandwidth, the fabrication process of this actuation layer requires complex multi-step processing to ensure a crack-free deposition of the piezoelectric material [38] and is not commonly offered by commercial foundries. Therefore, the production scalability of devices with a piezoelectric coating is currently limited. Conversely, auxiliary laser heating requires no additional layer stack to act on f_{rep} , and thus offers a much simpler alternative for active f_{rep} stabilization. By regulating the auxiliary laser frequency (f_{aux}), the detuning between the auxiliary laser and its corresponding resonance can be adjusted, which in turn regulates the intra-cavity power contribution. Consequently, the cavity-pump detuning changes and the auxiliary laser establishes an active control over f_{rep} . This approach thus combines the ease of stably accessing the parameter range, within which stable solitons exist, with the benefit of providing an independent pathway for f_{rep} stabilization.

To control f_{rep} using this approach, the actuation characteristics must be known. In this work, we examined the relation between f_{rep} and f_{aux} using a telecommunication C-band auxiliary laser. First, we obtained a bright soliton with a broad spectral bandwidth by launching the pump and the auxiliary lasers in orthogonal polarizations from counter-propagating directions. Next, we modulated f_{aux} at different modulation rates and recorded the response of f_{rep} to variations in f_{aux} . We find that f_{rep} varies linearly with f_{aux} within the modulation bandwidth of our auxiliary laser. Thus, f_{aux} can be deployed as an active linear feedback actuator to stabilize the microcomb. In addition, the linear variation of f_{rep} with f_{aux} makes it possible to precisely sweep the repetition rate for optical ranging measurements [40]. We further studied the effectiveness of the scheme by measuring the change in the variation ratio of f_{rep} with respect to f_{aux} at different modulation frequencies (f_{mod}). We used the variation ratio, defined as the ratio of the change in f_{rep} to the change in f_{aux} , to determine the impact of the auxiliary laser drift on f_{rep} . We found that, below a 1-kHz offset from the carrier, the repetition rate phase noise of the microcomb is dominated by the drift of f_{aux} .

2. Device and experimental setup

For this study, we used an Si₃N₄ microring resonator with a radius of 228 μm that was fabricated by Ligentec, a commercial foundry, as our nonlinear material platform. We used a thermoelectric cooler (TEC) underneath the substrate of the microresonator to stabilize the operating temperature of the device and thereby minimized the cavity resonance drift due to fluctuations in the temperature of the surroundings. The cross-section of the microring resonator is 1550 nm × 800 nm. We used a straight waveguide of similar cross-section for coupling light in/out of the resonator. The measured loaded quality factor (Q_L) and free spectral range (FSR) of the fundamental TE mode were 2.1×10^6 and 99.8 GHz respectively at 1552.8 nm, which is the pump wavelength (λ_p) in this study. We coupled the auxiliary laser into the fundamental TM mode at 1543.6 nm (λ_{aux}); the Q_L at λ_{aux} was 1×10^6 . We used a Michelson fiber interferometer of FSR 33.2 MHz at 1550 nm to characterize the transmission spectrum at λ_p and λ_{aux} with a Lorentzian lineshape fit for the Q -measurements [Fig. 1(a-b)]. We found the anomalous dispersion profile of the device by

measuring the integrated dispersion (D_{int}) of the fundamental TE mode family, which we then fit with a parabola [Fig. 1(c)]. From the parabolic fitting, we estimated the second-order dispersion $D_2/2\pi$ to be 1.46 MHz, which corresponds to a group velocity dispersion of $-155.4 \text{ ps}^2/\text{km}$.

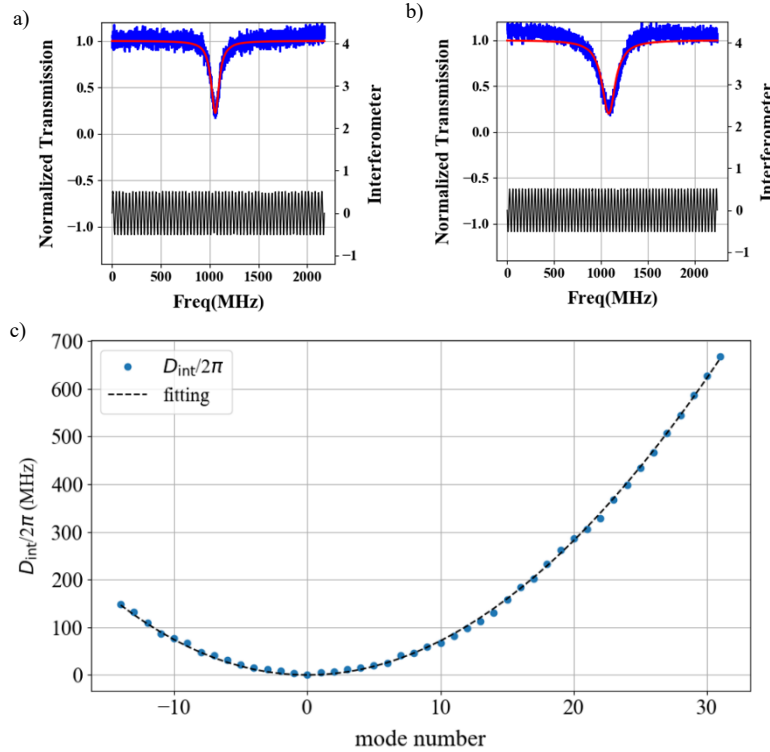


Fig. 1. Characterization of Si_3N_4 microresonator device. (a) Q -measurement of the fundamental (a) TE mode at 1552.8 nm and (b) TM mode at 1543.6 nm. The upper traces in (a) and (b) show the transmission spectrum in blue and the corresponding Lorentzian lineshape fit in red. The lower trace in black is the response of a Michelson interferometer to the laser frequency sweep. (c) Integrated dispersion (D_{int}) measurement of the fundamental TE mode family. The dotted line is the parabolic fit of D_{int} .

In Fig. 2, we show the experimental setup for the soliton microcomb generation and measurement of f_{rep} as f_{aux} varies. The pump laser was a tunable external-cavity diode laser (ECDL, Santec TSL-770) operating at λ_p . The auxiliary laser, operating at λ_{aux} , was also an ECDL (Newport TLB-6728), which has a modulation bandwidth of 2 kHz. We used an arbitrary function generator (AWG, Keysight 33500B) to modulate the frequency of the auxiliary laser to study the tuning of f_{rep} . Next, we coupled a small portion (7%) of the auxiliary laser output into the Michelson fiber interferometer to determine the variation of f_{aux} in response to the frequency modulation input from AWG to the TLB-6728 ECDL piezo controller. The pump and the auxiliary lasers were then amplified and coupled into the device in counter-propagating directions using tapered lensed fibers. We used a pair of polarization controllers (PCs) to adjust the launch conditions into the fundamental TE- and TM-modes at λ_p and λ_{aux} respectively. The circulators, located before the tapered lensed fibers, isolated the forward-propagating pump/soliton microcomb and the counter-propagating auxiliary laser/four-wave mixing (FWM) comb. To compensate the intracavity power drop during the soliton formation, the device required that the coupled power into the resonance at λ_{aux} surpasses the parametric oscillation threshold and hence the

FWM comb formed in the counter-propagating direction. In the forward-propagating direction, we used a portion of the light to capture the spectrum of the soliton comb using an optical spectrum analyzer (OSA) and routed the rest of the light to a pair of tunable fiber Bragg grating (FBG) notch filters to suppress λ_p and λ_{aux} . We monitored the transmission power at λ_p using a low-speed photodetector (PD1, 3-dB bandwidth 125 MHz) and an oscilloscope. The filtered comb was directed to a lithium-niobate electro-optic modulator (EOM) to detect f_{rep} using the method described in [35]. A second low-speed photodetector (PD2, 3-dB bandwidth 20 GHz) detected the beat note (f_{beat}) generated by EOM sidebands from the neighboring comb modes. Subsequently, we routed a portion of the detected RF signal to an electrical spectrum analyzer (ESA) and down converted the remainder of the signal using a broadband mixer, a local oscillator (LO) and a 1:128 pre-scaler chain before entering the phase noise measurement system (PNMS, Microchip 53100A). The frequency of the LO signal at the mixer was 29.8 GHz, which was provided from a second signal generator (Anritsu 3679C, Single sideband phase noise – 94 dBc/Hz at a 1-kHz offset).

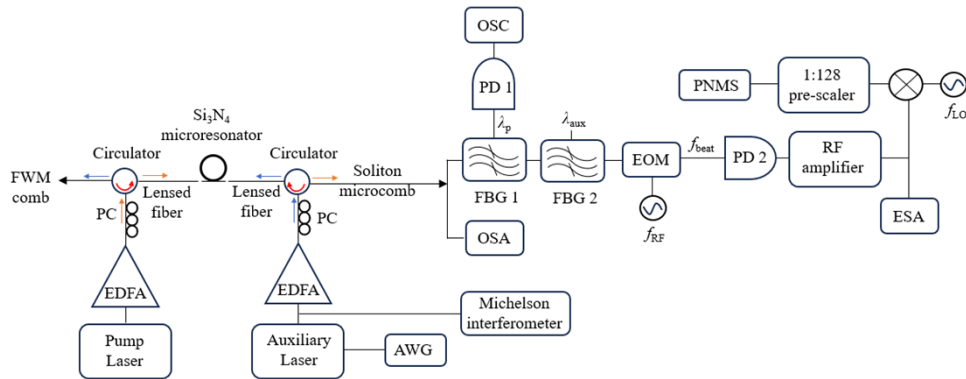


Fig. 2. A Schematic illustration of the experimental setup. FWM: Four-Wave Mixing; PC: Polarization Controller; EDFA: Erbium-Doped Fiber Amplifier; AWG: Arbitrary Function Generator; OSA: Optical Spectrum Analyzer; FBG: Fiber Bragg Grating filter; λ_p : Pump laser wavelength; λ_{aux} : Auxiliary laser wavelength; PD: Photo Detector; OSC: Oscilloscope; EOM: Electro-Optic Modulator; f_{RF} : Frequency of the RF signal driving the EOM; f_{beat} : Frequency of the beat note; f_{LO} : Frequency of the Local Oscillator at the RF mixer; ESA: Electrical Spectrum Analyzer; PNMS: Phase Noise Measurement System

3. Results and discussion

We generated the soliton microcomb by slowly tuning λ_p to the red-detuned side of the pump resonance at 1552.8 nm. The soliton step size was optimized by placing λ_{aux} on the thermally stable, blue-detuned side of the corresponding resonance at 1543.6 nm and adjusting the auxiliary laser power to balance the abrupt intracavity power drop during the soliton transitions. Figure 3 shows the optical spectrum and the hyperbolic-secant-squared spectral envelope of the generated single soliton microcomb spanning over 100 nm. The forward-propagating pump was launched at 270 mW into the waveguide, while the counter-propagating auxiliary laser was operating at 270.2 mW. The spectral maximum of the soliton comb shows a large negative frequency shift with respect to λ_p . Such a spectral redshift, often observed in amorphous silica- and Si_3N_4 -based microresonator devices, occurs due to the presence of the Raman effect and a dispersive wave (DW) [41]. DWs may appear due to the presence of a higher-order dispersion in the device. They can also occur due to an avoided mode crossing between the soliton generating mode family and a cavity mode from another mode family. The integrated dispersion (D_{int}) measurement

of the fundamental TE-mode [Fig. 1(c)] shows no signs of presence of strong higher-order dispersion, rather demonstrates a pure anomalous GVD profile. The smooth symmetric soliton comb spectral envelope also indicates that no significant higher-order dispersion effect is present [42]. Furthermore, the resonances from higher order mode families, that can cause an avoided mode-crossing, were not observed in the transmission spectra during the D_{int} measurement and in the D_{int} profile of the fundamental TE-mode. Hence, we attribute this large negative frequency shift to the Raman-induced soliton self-frequency shift (SSFS), the magnitude of which increases with the bandwidth of the soliton microcomb [43].

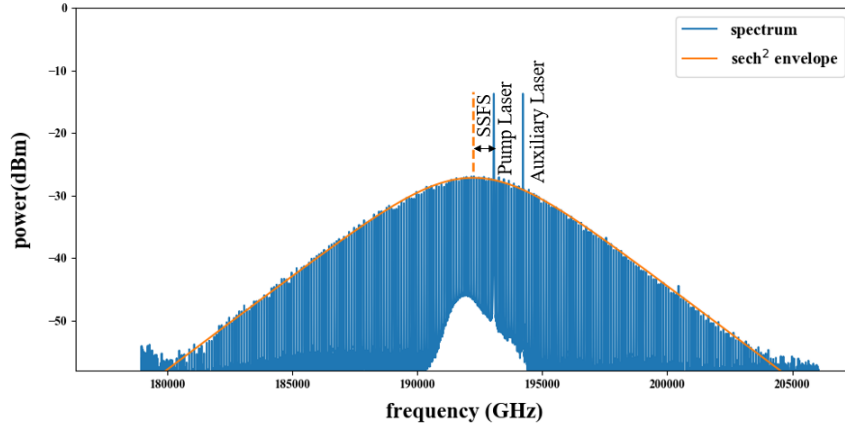


Fig. 3. Single soliton microcomb spectrum at the OSA, SSFS: Soliton Self-Frequency Shift.

We found the repetition rate (f_{rep}) of the generated microcomb using f_{beat} as illustrated in Fig. 4(a). The RF port of the lithium niobate EOM was driven by a 40-GHz tone (f_{RF}), which generates the first order sidebands from the comb lines and allowed us to relate f_{rep} to the beat note via the relation $f_{\text{beat}} = f_{\text{rep}} - 2 \times f_{\text{RF}}$. Figure 4(b) shows the electrical spectrum of f_{beat} , which is centered at 19.8 GHz (corresponding to $f_{\text{rep}} = 99.8$ GHz) and that we measured using an ESA with a resolution bandwidth of 30 kHz.

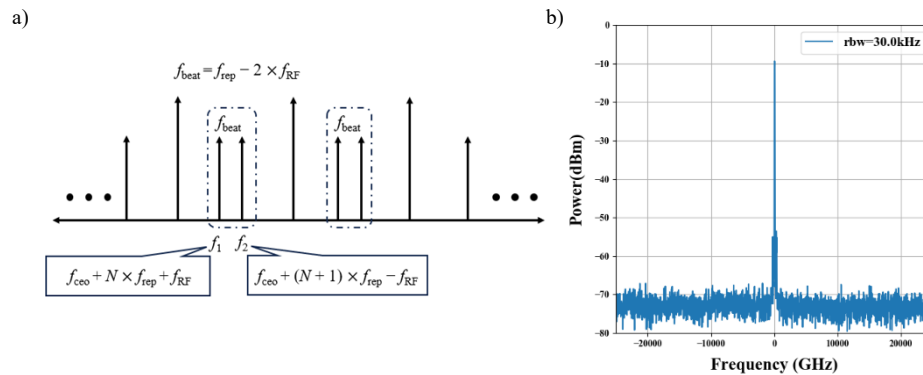


Fig. 4. Repetition rate (f_{rep}) detection. (a) the detection scheme using the EOM and f_{beat} . (b) the detected f_{rep} spectrum at ESA where $f_{\text{rep}} = f_{\text{beat}} + 2 \times f_{\text{RF}}$

Next, we studied the sensitivity of f_{rep} of the generated soliton comb by providing a frequency modulation input to the piezo controller of the TLB-6728 auxiliary laser unit. The frequency

modulation input, generated by the AWG, was a triangle waveform of frequency, f_{mod} . As we modulated the f_{aux} , we monitored the transmission power at λ_p on the oscilloscope to ensure that the intracavity power contribution by the auxiliary laser does not overcompensate any thermal drift and thereby excites multi-solitons in the cavity [44]. We measured the variations of f_{aux} at different modulation frequencies (f_{mod}) using the Michelson interferometer, as shown in Fig. 2. The ESA, operating in max-hold mode, captured the corresponding f_{rep} variations. Figure 5(a) shows the maximum f_{rep} variation with respect to the maximum f_{aux} variation at $f_{\text{mod}} = 100$ Hz and $f_{\text{mod}} = 1$ kHz. As the f_{aux} variation increases, the f_{rep} variation increases linearly due to an interplay between the intracavity power change and cavity temperature shift. With the variation in f_{aux} , the detuning between the auxiliary laser and corresponding resonance changes, which in turn shifts the intracavity power dynamics. As the detuning increases, the intracavity power contribution by the auxiliary laser decreases, which causes a cavity temperature drop and vice versa. Consequently, the resonator FSR changes due to the thermo-optic effect, which in turn directly leads to a change in f_{rep} . The FSR change also induces a change in the cavity-pump detuning, so that the Raman-induced soliton self-frequency shift (SSFS) also varies with the f_{aux} modulation. Since the SSFS is also linearly related to f_{rep} , both effects contribute to linear actuation of f_{rep} by tuning f_{aux} . We note that in resonators where a dispersive wave appears, the resulting soliton recoil may lead to a nonlinear relation between f_{rep} and the cavity-pump detuning, and hence may lead to nonlinear features in the control of f_{rep} by f_{aux} [45]. In our resonator, we confirmed that no dispersive wave appears.

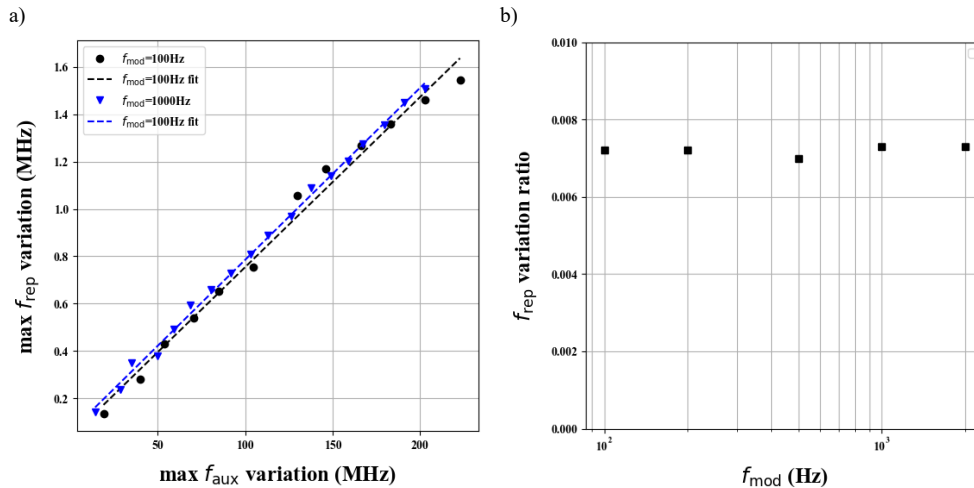


Fig. 5. Characteristics of the linear feedback actuator of the repetition rate (f_{rep}). (a) The sensitivity of f_{rep} varies linearly with f_{aux} . (b) the f_{rep} variation ratio remains unchanged with higher f_{mod} .

We investigated the sensitivity of f_{rep} at different modulation frequencies (f_{mod}) by estimating f_{rep} variation ratio, which we defined as the ratio between the max f_{rep} variation in MHz and the max f_{aux} variation in MHz at f_{mod} . The f_{rep} variation ratio indicates the effectiveness of the applied f_{aux} actuation on f_{rep} of the soliton microcomb. Figure 5(b) shows the variation ratio of f_{rep} with respect to f_{mod} . For the device we used in this study, the variation ratio did not change within the adjustable bandwidth of the auxiliary laser. The variation ratio also correlates the auxiliary laser phase fluctuation ($\Delta\phi_{\text{aux}}$) to the repetition rate phase fluctuation $\Delta\phi_{\text{rep}}$ via the relation $\Delta\phi_{\text{rep}} = (\Delta f_{\text{rep}}/\Delta f_{\text{aux}}) \times \Delta\phi_{\text{aux}}$. Since f_{rep} varies linearly with f_{aux} , as shown in Fig. 5(a), the impact of the phase fluctuation of the auxiliary laser light on the repetition rate phase noise

scales at $\langle \text{variation ratio}^2 \rangle$ in our system. To determine this contribution, we analyzed the phase noise of the auxiliary laser and the repetition rate of the microcomb using the phase noise measurement system (PNMS, Microchip 53100A).

After generating the soliton microcomb [Fig. 3] and subsequently detecting the repetition rate [Fig. 4], we mixed a portion of f_{beat} with a 29.8 GHz RF signal (f_{LO}) to down-convert the beat note to a 10-GHz RF signal. Next, we used a series of pre-scalers to divide the frequency of the down-converted beat note by a factor of 128 to operate within the frequency range of our PNMS (frequency range limited to 200 MHz). Figure 6 shows the single sideband (SSB) phase noise measurements of the RF signal scaled at 99.8 GHz (f_{rep} , blue trace) and the noise-floor (gray trace) of the repetition rate detection subsystem that includes the mixer and the pre-scaler chain. We measured the noise floor by modulating the pump laser at λ_p using the same EOM and RF driver, used for f_{rep} detection, and then mixing with f_{LO} before passing through the 1:128 pre-scaler chain. The noise-floor of the subsystem was 55 dB below the SSB phase noise measurement of the free-running soliton microcomb at 1-kHz offset. We then measured the phase noise of the auxiliary laser using the delayed self-heterodyne interference technique with a fiber-optic Michelson interferometer [46]; the path length difference between the two arms of the interferometer was 6 m. We used the first order diffracted beam from the acousto-optic modulator (AOM) to achieve 110 MHz frequency shift of the auxiliary laser light on the AOM-arm of the Michelson Interferometer and used the PNMS to measure the phase noise of the beat signal detected using a low-speed photodetector (3-dB bandwidth 20 GHz). We then took account of the transfer function of the interferometer to estimate the phase-noise of the auxiliary laser, $\mathcal{L}_{\text{aux}}(f)$ from the measured phase noise of the beat signal, $\mathcal{L}_{\text{beat}}(f)$ using the expression, $\mathcal{L}_{\text{aux}}(f) = \frac{1}{4 \sin^2(\pi f \tau)} \mathcal{L}_{\text{beat}}(f)$, where f and τ refer to the offset frequency from the carrier and the time delay of the interferometer due the path length difference between the two arms [47].

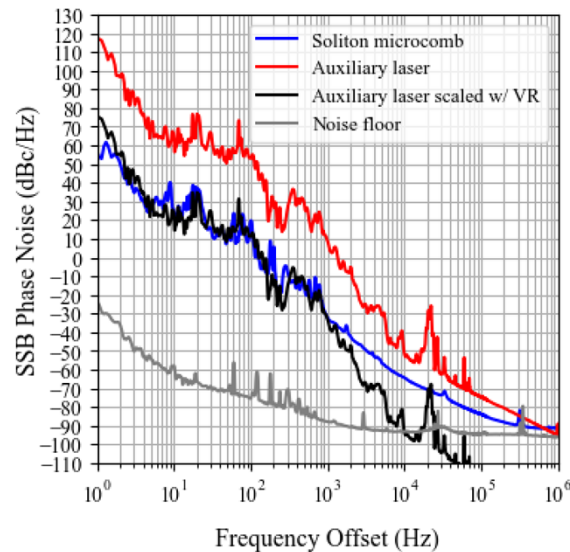


Fig. 6. Single sideband (SSB) phase noise measurements. The blue trace represents the phase noise of the repetition rate (f_{rep}) evaluated at 99.8 GHz in the free-running condition. The red (black) trace represents the auxiliary laser phase noise measured using the delayed self-heterodyne interference technique (scaled with VR: variation ratio). The gray trace represents the noise floor of the f_{rep} detection sub-system.

The red trace in Fig. 6 shows the SSB phase noise measurement of the auxiliary laser, which is then transposed using the scaling factor of $\langle \text{variation ratio}^2 \rangle$ (black trace). We found that the black trace coincides with the repetition rate phase noise measurement (blue trace) below a 1-kHz offset from the carrier. This overlapping occurs due to the prevailing correlation between the phase fluctuation of the auxiliary laser and cavity-pump detuning. When the phase of the auxiliary laser drifts, the intracavity power drifts as well. Consequently, the cavity-pump detuning shifts in response to the thermal heating/cooling due to the cavity temperature variation and the phase instability in the repetition rate occurs. The extent of the phase fluctuation depends on the volume of the propagating mode, which the auxiliary laser light is coupled into, and the thermal responsivity of the device. As shown in Fig. 6, the phase noise of the auxiliary laser in our setup sets a limit on the phase noise performance of the free-running soliton repetition rate below a 1-kHz offset from the carrier. The result indicates that the phase stability of the repetition rate can be improved by using an inherently low-phase-noise auxiliary laser. The result also implies that it is necessary to lock the laser to a stable reference when the auxiliary laser heating technique is used only for aiding the DKS microcomb formation in the system. At offset frequencies greater than 1 kHz, the auxiliary laser frequency noise term no longer dominates the phase noise. Many other noise sources may contribute to the noise in f_{rep} . For example, f_{rep} noise can arise from fluctuations in the cavity-pump detuning, which may be caused by instability in the pump laser frequency [31] or by transduction of intracavity power fluctuations into the cavity-pump detuning fluctuations via the Kerr nonlinearity [3]. Hence, further investigation is required to determine the underlying noise source(s) of the phase instability in f_{rep} at offset frequencies greater than 1 kHz.

4. Conclusions

To summarize, we examine the tuning of the repetition rate (f_{rep}) of a bright soliton microcomb using the auxiliary laser heating technique and probe the role of an auxiliary laser as an f_{rep} actuator. We also analyze the effect of the phase fluctuation of the auxiliary laser on f_{rep} when this technique is used to facilitate the soliton microcomb generation alone. We investigate the characteristics of f_{rep} actuation by modulating the frequency of the auxiliary laser (f_{aux}) and show that f_{rep} varies linearly with f_{aux} within the thermal response time of the cavity. Consequently, one can use the correlation between f_{rep} and f_{aux} to implement a linear active feedback actuator by regulating f_{aux} via an error signal corresponding to the f_{rep} fluctuation. The error signal can be obtained by sending the detected f_{rep} signal to a phase comparator with a stable reference. It thus offers an independent “knob” for microcomb stabilization and reduces the dependence on the pump laser. Although the additional components required to implement the auxiliary laser technique add complexity to the comb generation system, the simplicity of soliton generation as well as the additional tuning knob may outweigh this downside in some applications. Furthermore, when both the pumped and the auxiliary resonance modes have sufficiently high Q s, the pump as well as the auxiliary laser require no optical amplification to operate at the necessary power levels and the implementation architecture becomes simpler [21]. A feedback actuation using this technique is particularly important in constraint conditions, such as an additional actuation layer is unavailable due to fabrication limitations, or an effective actuation bandwidth is unattainable due to lack of efficiency. However, there exists a trade-off that stems from the inherent phase-noise of the auxiliary laser. The phase noise of the auxiliary laser directly influences the intracavity power dynamics and thereby varies the detuning between the pump and the pumped cavity resonance, which causes f_{rep} fluctuation. Consequently, the phase variation of the auxiliary laser can degrade the phase stability of the microcomb. We find that the phase noise of the auxiliary laser in our setup dominates the phase noise of f_{rep} below a 1-kHz offset from the carrier. In this case, the phase noise performance of f_{rep} can in principle be improved by stabilizing the auxiliary laser after the microcomb generation is completed. Since our focus in this paper is the demonstration

that f_{aux} is suitable as a linear feedback actuator, the auxiliary laser in our setup is not locked to a stable reference.

Funding. U.S. Department of Defense (HQ0034-20-2-0007).

Acknowledgments. The authors would like to thank Dr. Xu Yi, Associate Professor of Physics at University of Virginia and Dr. Alioune Niang, post-doctoral research associate at University of Maryland, Baltimore County for technical assistance and insightful discussion.

Work at UMBC was supported by collaborative agreements 2022138-142232 and 2023200-142386 with the National Center for Manufacturing Sciences as a sub-award from US DoD cooperative agreement HQ0034-20-2-0007.

Disclosures. The authors declare no conflict of interest.

Data availability. Data underlying the results presented in this paper are not publicly available at this time but may be obtained from the authors upon reasonable request.

References

1. X. Yi, Q.-F. Yang, K. Y. Yang, *et al.*, “Soliton frequency comb at microwave rates in a high-Q silica microresonator,” *Optica* **2**(12), 1078–1085 (2015).
2. P. Del’Haye, A. Coillet, W. Loh, *et al.*, “Phase steps and resonator detuning measurements in microresonator frequency combs,” *Nat. Commun.* **6**, 5668 (2015).
3. J. R. Stone, T. C. Briles, T. E. Drake, *et al.*, “Thermal and nonlinear dissipative-soliton dynamics in Kerr-microresonator frequency combs,” *Phys. Rev. Lett.* **121**(6), 063902 (2018).
4. B. Shen, L. Chang, J. Liu, *et al.*, “Integrated turnkey soliton microcombs,” *Nature* **582**(7812), 365–369 (2020).
5. V. Brasch, M. Geiselmann, T. Herr, *et al.*, “Photonic chip-based optical frequency comb using soliton Cherenkov radiation,” *Science* **351**, 357–360 (2015).
6. Q. Li, T. C. Briles, D. A. Westly, *et al.*, “Stably accessing octave-spanning microresonator frequency combs in the soliton regime,” *Optica* **4**(2), 193–203 (2017).
7. X. Ji, F. A. S. Barbosa, S. P. Roberts, *et al.*, “Ultra-low-loss on-chip resonators with sub-milliwatt parametric oscillation threshold,” *Optica* **4**(6), 619–624 (2017).
8. C. Bao, Y. Xuan, J. A. Jaramillo-Villegas, *et al.*, “Direct soliton generation in microresonators,” *Opt. Lett.* **42**(13), 2519–2522 (2017).
9. T. Herr, V. Brasch, J. D. Jost, *et al.*, “Temporal solitons in optical microresonators,” *Nat. Photonics* **8**(2), 145–152 (2014).
10. L. Chang, W. Xie, H. Shu, *et al.*, “Ultra-efficient frequency comb generation in AlGaAs-on-insulator microresonators,” *Nat. Commun.* **11**, 1331 (2020).
11. L. Wu, W. Xie, H.-J. Chen, *et al.*, “AlGaAs soliton microcombs at room temperature,” *Opt. Lett.* **48**(15), 3853–3856 (2023).
12. H. Jung, S.-P. Yu, D. R. Carlson, *et al.*, “Tantala Kerr nonlinear integrated photonics,” *Optica* **8**(6), 811–817 (2021).
13. H. Jung, C. Xiong, K. Y. Fong, *et al.*, “Optical frequency comb generation from aluminum nitride microring resonator,” *Opt. Lett.* **38**(15), 2810–2813 (2013).
14. X. Liu, Z. Gong, A. W. Bruch, *et al.*, “Aluminum nitride nanophotonics for beyond-octave soliton microcomb generation and self-referencing,” *Nat. Commun.* **12**, 5428 (2021).
15. L. Chang, S. Liu, and J. E. Bowers, “Integrated optical frequency comb technologies,” *Nat. Photonics* **16**(2), 95–108 (2022).
16. A. A. Savchenkov, V. S. Ilchenko, F. D. Teodoro, *et al.*, “Generation of Kerr combs centered at 4.5 μm in crystalline microresonators pumped with quantum-cascade lasers,” *Opt. Lett.* **40**(15), 3468–3471 (2015).
17. D. T. Spencer, T. Drake, T. C. Briles, *et al.*, “An optical-frequency synthesizer using integrated photonics,” *Nature* **557**(7703), 81–85 (2018).
18. J. Liu, E. Lucas, A. S. Raja, *et al.*, “Photonic microwave generation in the X- and K-band using integrated soliton microcombs,” *Nat. Photonics* **14**(8), 486–491 (2020).
19. C. Godey, I. V. Balakireva, A. Coillet, *et al.*, “Stability analysis of the spatiotemporal Lugiato-Lefever model for Kerr optical frequency combs in the anomalous and normal dispersion regimes,” *Phys. Rev. A* **89**(6), 063814 (2014).
20. C. Joshi, J. K. Jang, K. Luke, *et al.*, “Thermally controlled comb generation and soliton modelocking in microresonators,” *Opt. Lett.* **41**(11), 2565–2568 (2016).
21. S. Zhang, J. M. Silver, L. D. Bino, *et al.*, “Sub-milliwatt-level microresonator solitons with extended access range using an auxiliary laser,” *Optica* **6**(2), 206–212 (2019).
22. H. Zhou, Y. Geng, W. Cui, *et al.*, “Soliton bursts and deterministic dissipative Kerr soliton generation in auxiliary-assisted microcavities,” *Light: Sci. Appl.* **8**, 50 (2019).
23. H. Weng, J. Liu, A. A. Afridi, *et al.*, “Directly accessing octave-spanning dissipative Kerr soliton frequency combs in an AlN microresonator,” *Photonics Res.* **9**(7), 1351–1357 (2021).
24. H. Weng, A. A. Afridi, J. Li, *et al.*, “Dual-mode microresonators as straightforward access to octave-spanning dissipative Kerr solitons,” *APL Photonics* **7**(6), 066103 (2022).
25. J. D. Jost, E. Lucas, T. Herr, *et al.*, “All-optical stabilization of a soliton frequency comb in a crystalline microresonator,” *Opt. Lett.* **40**(20), 4723–4726 (2015).

26. R. Niu, S. Wan, S.-M. Sun, *et al.*, “Repetition rate tuning and locking of solitons in a microrod resonator,” *Opt. Lett.* **49**(3), 570–573 (2024).
27. T. E. Drake, J. R. Stone, T.C. Briles, *et al.*, “Thermal decoherence and laser cooling of Kerr microresonator solitons,” *Nat. Photonics* **14**(8), 480–485 (2020).
28. G. Moille, J. Stone, M. Chojnacky, *et al.*, “Kerr-induced synchronization of a cavity soliton to an optical reference,” *Nature* **624**(7991), 267–274 (2023).
29. T. Wildi, A. Ulanov, N. Englebert, *et al.*, “Sideband injection locking in microresonator frequency combs,” *APL Photonics* **8**, 120801 (2023).
30. J. K. Jang, X. Ji, C. Joshi, *et al.*, “Observation of Arnold tongues in coupled soliton Kerr frequency combs,” *Phys. Rev. Lett.* **123**, 153901 (2019).
31. X. Yi, Q. F. Yang, K. Y. Yang, *et al.*, “Active capture and stabilization of temporal solitons in microresonators,” *Opt. Lett.* **41**(9), 2037–2040 (2016).
32. S. Fujii, K. Wada, R. Sugano, *et al.*, “Versatile tuning of Kerr soliton microcombs in crystalline microresonators,” *Commun. Phys.* **6**, 1 (2023).
33. I. R. Salgado, Ó. B. Helgason, V. Durán, *et al.*, “Active feedback stabilization of super-efficient microcombs in photonic molecules,” *Opt. Lett.* **49**, 2325–2328 (2024).
34. D. Kwon, D. Jeong, I. Jeon, *et al.*, “Ultrastable microwave and soliton-pulse generation from fibre-photonic-stabilized microcombs,” *Nat. Commun.* **13**, 381 (2022).
35. P. Del’Haye, S. B. Papp, and S. A. Diddams, “Hybrid electro-optically modulated microcombs,” *Phys. Rev. Lett.* **109**(26), 263901 (2012).
36. X. Xue, Y. Xuan, C. Wang, *et al.*, “Thermal tuning of Kerr frequency combs in silicon nitride microring resonators,” *Opt. Express* **24**(1), 687–698 (2016).
37. J. Liu, H. Tian, E. Lucas, *et al.*, “Monolithic piezoelectric control of soliton microcombs,” *Nature* **583**(7816), 385–390 (2016).
38. W. Jin, R. G. Polcawich, P. A. Morton, *et al.*, “Piezoelectrically tuned silicon nitride ring resonator,” *Opt. Express* **26**(3), 3174–3187 (2018).
39. S. B. Papp, P. Del’Haye, and S. A. Diddams, “Mechanical control of a microrod-resonator optical frequency comb,” *Phys. Rev. X* **3**, 031003 (2013).
40. J. Zheng, Y. Wang, X. Wang, *et al.*, “Optical ranging system based on multiple pulse train interference using soliton microcomb,” *Appl. Phys. Lett.* **118**(26), 261106 (2021).
41. M. Karpov, H. Guo, A. Kordts, *et al.*, “Raman self-frequency shift of dissipative Kerr solitons in an optical microresonator,” *Phys. Rev. Lett.* **116**(10), 103902 (2016).
42. N. Akhmediev and M. Karlsson, “Cherenkov radiation emitted by solitons in optical fibers,” *Phys. Rev. A* **51**(3), 2602–2607 (1995).
43. Q.-F. Yang, X. Yi, K. Y. Yang, *et al.*, “Spatial-mode-interaction-induced dispersive waves and their active tuning in microresonators,” *Optica* **3**(10), 1132–1135 (2016).
44. H. Weng, M. McDermott, A. A. Afridi, *et al.*, “Turn-key Kerr soliton generation and tunable microwave synthesizer in dual-mode Si₃N₄ microresonators,” *Opt. Express* **32**(3), 3123–3137 (2024).
45. X. Yi, Q. F. Yang, X. Zhang, *et al.*, “Single mode dispersive waves and soliton microcomb dynamics,” *Nat. Commun.* **8**, 14869 (2017).
46. A. Canagasabey, A. Michie, J. Canning, *et al.*, “A Comparison of delayed self-heterodyne interference measurement of laser linewidth using Mach-Zehnder and Michelson interferometers,” *Sensors* **11**(10), 9233–9241 (2011).
47. S. Camatel and V. Ferrero, “Narrow linewidth CW laser phase noise characterization methods for coherent transmission system applications,” *J. Lightwave Technol.* **26**(17), 3048–3055 (2008).